BUCKLING FAILURE OF CANTILEVER TYPE CYLINDRICAL SHELLS UNDER THE HORIZONTAL LOAD

by

M.Yoneda,[I)] H.Ohmori[I)] and Y.Hangai[I)]

INTRODUCTION

It is reported that many liquid-storage tanks were damaged by buckling in Sendai, Japan during the June 1978 earthquake [1] as well as in Livermore, California during the Greenvill-Mt.Diabo earthquake of January 24, 1980 [2]. As shown in these damages, the buckling problem of tower-shaped cylindrical shells subjected to earthquake excitation is of practical importance in the design of liquid-storage tanks, silos, etc. Stress distributions obtained by the linear analysis show very complicated combination of axial compression, bending and shear, and in addition are influenced strongly by the change of a height-to-diameter ratio (H/D). Since these stress distributions govern mainly the pre-buckling state of stress, the buckling behaviour of cylindrical shells due to the horizontal load is more complicated than, for example, one of the uniformly pressurized cylindrical shell. On the basis of the above perspective, a test program which has the following distinctive features was set up: (1) test for a large number of test cylinders in order to investigate statistically and (2) use of the loading apparatus of displacement control type in order to grasp the behaviours in the vicinity of the buckling point, even in the unstable equilibrium condition.

Untill now we have tested about 110 cylinders for three kinds of boundary condition, and in this paper, we present the test results for 34 test cylinders of the same dimension as well as of the same boundary condition.

TEST CYLINDER AND LOADING APPARATUS

An aluminum can with the dimension of radius: R=3.3cm, height: H=9.4cm and thickness: t=0.015cm is adopted for test cylinder (see Fig.1). Hence the shape parameters H/D and t/R are about 1.42 and 1/200, respectively. Distribution of thickness on the overall surface for a typical cylinder is measured to estimate the imperfection of thickness. The result is given in Table-1. In order to obtain the material properties of test cylinders, the tensile loading test for two kinds of test specimen, which are cutted out along the longitudinal direction and the circumferential one, respectively, as shown in Fig.1, was carried out. An example of typical stress-strain relations is depicted in Fig.2 and the elastic properties such as Young's modulus and Poisson's ratio are tabulated in Table-2.

Two sets of boundary conditions which are shown in Fig.3 are considered; (a) both ends clamped; or (b) one end clamped and the other free. In addition, in the case of (b), circular configuration of the top end is always kept by the steel cap in order to model the effect of ring girder which is usually attached.

I) Institute of Industrial Science, University of Tokyo

A loading apparatus which can control the displacement of the top cap by turning the screw bar was developed for this test. Load level can be automatically recorded by a load cell attached to the end of the screw bar (see Fig.4). Key of this apparatus is that any prescribed displacement may be settled, even in the unstable equilibrium condition near the buckling points, to measure displacements and strains on the surface.

STRESS DISTRIBUTIONS BY THE LINEAR ANALYSIS

In order to examine stress distributions in the pre-buckling state, the linear analysis was carried out by using the governing equations of Donnel type, whose nondimensionalized form are

$$\begin{aligned}
&[\nabla^8+\frac{\partial^4}{\partial\theta^4}\{(2+\nu)\frac{\partial^2}{\partial\xi^2}+\frac{\partial^2}{\partial\theta^2}\}+\beta^4\frac{\partial^4}{\partial\xi^4}]w=0\\
&\nabla^4 u-\frac{\partial}{\partial\xi}(\frac{\partial^2}{\partial\theta^2}-\nu\frac{\partial^2}{\partial\xi^2})w=0\\
&\nabla^4 v+\frac{\partial}{\partial\theta}\{(2+\nu)\frac{\partial^2}{\partial\xi^2}+\frac{\partial^2}{\partial\theta^2}\}w=0
\end{aligned} \qquad (1)$$

where $\nabla^2=\partial^2/\partial\xi^2+\partial^2/\partial\theta^2$, $\nabla^4=\nabla^2\nabla^2$, $\nabla^8=\nabla^4\nabla^4$, and nondimensional coordinates ξ, θ and displacements u,v,w are defined by $\xi=x/R$, $\theta=s/R$, $u=\bar{u}/R$, $v=\bar{v}/R$, $w=\bar{w}/R$, respectively. The coefficient β has the relation of $\beta^4=12(1-\nu^2)(R/t)^2$. Moreover, displacements u,v,w are assumed to have the form

$$\begin{aligned}
u(\xi,\theta)&=U(\xi)\cos(n\theta) \quad , \quad U(\xi)=Be^{p\xi}\\
v(\xi,\theta)&=V(\xi)\sin(n\theta) \quad , \quad V(\xi)=Ce^{p\xi}\\
w(\xi,\theta)&=W(\xi)\cos(n\theta) \quad , \quad W(\xi)=Ae^{p\xi}
\end{aligned} \qquad (2)$$

Numerical analysis was performed by means of the Hoff's method under the condition that the top end of the cylindrical shell was enforced to have an unity horizontal displacement according to the Fourier expansion number of n=1. Concerning the boundary conditions, three sets which are shown in Fig.5 are considered. Dimensions and material properties used for numerical analysis are given in Fig.1. Magnitude of reaction, stress resultants Nx and Nsx, membrane principal stress and convergent behaviours of Ns and Mx under the enforcement of the unit displacement are shown in Fig.6.

The axial stress resultant Nx causes the buckling in the portion near the bottom edge which is similar to the diamond-shaped buckling, while the shear stress resultant Nsx results in the shear buckling being similar to a plate buckling due to shear. But in the short cylindrical shell, combined effect of these stresses is more important, especially for a tower-shaped cylindrical shell. This is understood from observing the principal stress flows in the shell which are shown in Fig.6. In the case of both ends clamped, all the stress resultants and stress couples are distributed symmetrically with respect to the circumferential line at the middle height. On the other hand, distribution of comparatively large principal stresses shifts to the lower part near the edge, so that buckling due to the combined load both of axial compressive stress and shear is apt

to occur. This situation is observed in the test (see Fig.9).

As for the convergent behaviour of the hoop stress Ns and bending moment Mx in the neighbourhood of the basement, the decay length $Lc=\pi\sqrt{Rt}/[3(1-\nu^2)]^{1/4}$, which is obtained for the circular cylindrical shell subjected only to axisymmetrical edge load, can be also applied to the cylindrical shell under the horizontal load, regardless of boundary condition, because the formula above gives us the Lc=0.058H for the shell considered here, while Fig.6 shows that Ns and Mx are almost converged at the point of 0.05H from the base.

Fig.7 represents comparisons of the maximum values about displacement, Nsx, Nx and M for the prescribed unit load. Maximum displacements and moments vary largely among the three cases, but maximum shears are almost the same. Maximum axial stress Nx for the cases (b) and (c) is twice as large as one for the case (a), which suggests that possibility of occurrence of the diamond-shaped buckling is higher for the cantilever type.

TEST RESULTS

Let us explain mainly the results of the cantilever-type test cylinder. The typical load-displacement curve at the top end of the shell is despicted in Fig.8, where at the point 1, the first dimple buckling occurs at the position shown in Fig.9(c). After that, the load decreases rapidly and then at the point 2 on the curve, the same type buckling appears in the opposite side of the first buckling on the shell surface. The difference between points 1 and 2, whose distribution is shown in Fig. 11, gives an index about various imperfection accompanyed with test. At the point 3, a diamond pattern appears at the lower part of the shell which is depicted as the number 3 in Fig.9(c), and after that, the load drops again suddenly to the stable equilibrium state whose load level is about 60-70 percent of the first buckling load.

The positions on the shell surface of dimple buckling modes are shown in Fig.9(a),(b) and (d). The first buckling modes gather in the middle line for the case of both ends clamped(a), while they moves a little to the lower part for the cantilever-type(b), because of the combined stress effect as mentioned in the previous section.

Relations between load and displacement for 34 test cylinders are plotted in Fig.10, which means a dispersion of the test results. It is shown that degree of scatter about the second shear-type buckling is large. Photo-1 shows the buckling modes appeared on a test cylinder.

CONCLUSION

This paper presents the test results in the first stage of the author's test programe on the buckling problem of the tower-shaped cylindrical shell under the earthquake excitation.

Let us here consider the buckling formula. The axial compression represented by Nx in the test is highly concentrated over the relatively narrow zone and causes a diamond-shaped dimple buckling just above the bottom edge at the point 3 in Fig.10. If the classical buckling formula for the axial compression

$$\sigma_{x_{cr}} = \frac{1}{\sqrt{3(1-\nu^2)}} \frac{Et}{R} \tag{3}$$

is applied to estimate the buckling stress in the narrow zone mentioned above, $\sigma x = 1.9 \times 10 kg/cm^2$ is obtained. This value leads to the horizontal load P=31.4kg by using the maximum value of Nx in Fig.7. Since this value is about 65 percent of the test result, the formula(3) cannot apply directly to the problem considered here and more investigation is necessary to recommend a simple formula.

REFERENCES

1) K.Kubo, et. al. "Miyagi-ken-oki Earthquake of June 12, 1978, Preliminary Report," "SEISAN-KENKYU" Monthly Journal of Institute of Industrial Science, University of Tokyo, Vol.30, No.11, Nov. 1978, pp.9-25.

2) "Greenville (Diablo-Livermore) Earthquake of January 1980: Reconnaissance Report," Earthquake Engineering Research Institute Newsletter, Vol.14, No.2, March 1980, pp.20-89.

3) K.Uchiyama, D.Yamada and K.Shiobara, "Buckling of Cylindrical Shells due to the Horizontal Load," Proc. Annual Convention of Architectural Institute of Japan, 1980, pp.1145-1146.

4) Clough, R.W., Niwa, A. and Clough, D.P., "Experimental Seismic Study of Cylindrical Tank," Proc. ASCE, Journal of the Structural Division, Vol.105, ST12, Dec. 1979, pp.2565-2590.

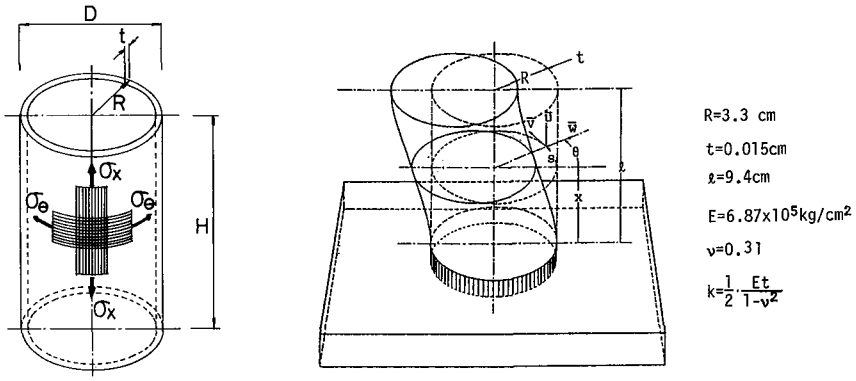

Fig.1: Cylindrical Shell due to Horizontal Load

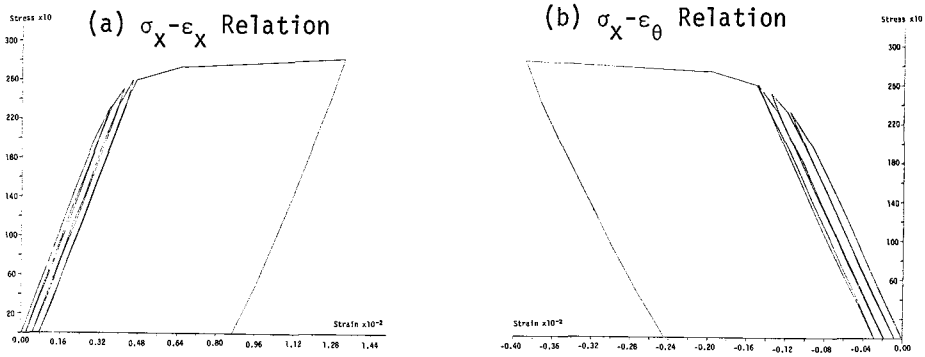

Fig.2: Stress-Strain Relation

(mm)

	1	2	3	4	5	6	7	8	9	10	11	12	Ave.
1	0.179	0.194	0.190	0.187	0.181	0.181	0.171	0.170	0.169	0.177	0.170	0.166	0.178
2	0.157	0.159	0.160	0.158	0.160	0.156	0.155	0.155	0.153	0.155	0.156	0.158	0.156
3	0.154	0.155	0.152	0.153	0.154	0.150	0.150	0.150	0.148	0.150	0.153	0.152	0.151
4	0.150	0.151	0.151	0.147	0.150	0.147	0.143	0.145	0.147	0.146	0.148	0.149	0.147
5	0.147	0.148	0.145	0.142	0.149	0.143	0.140	0.141	0.145	0.145	0.146	0.146	0.144
6	0.147	0.149	0.148	0.146	0.145	0.143	0.138	0.141	0.141	0.143	0.143	0.146	0.144
7	0.149	0.149	0.146	0.147	0.142	0.145	0.140	0.140	0.143	0.146	0.148	0.148	0.145
8	0.151	0.150	0.151	0.147	0.145	0.142	0.138	0.140	0.142	0.145	0.145	0.150	0.145
9	0.150	0.153	0.150	0.145	0.145	0.145	0.138	0.147	0.141	0.142	0.146	0.148	0.150
10	0.180	0.181	0.176	0.175	0.170	0.170	0.160	0.161	0.166	0.172	0.176	0.173	0.171
Ave.	0.156	0.158	0.156	0.154	0.154	0.152	0.147	0.149	0.149	0.152	0.153	0.153	0.153

Table 1: Distribution of Thickness on the Shell

	No.	Young's Modulus $10^5 kg/cm^2$	Poisson's Ratio
Longitudinal Direction	1	6.75	0.32
	2	6.72	0.30
	3	7.17	0.30
	4	6.84	0.31
Circumferential Direction	5	7.05	0.29
	6	6.84	0.33
	7	6.90	0.31
	8	6.72	0.31
Average		6.87	0.31

Table 2: Material Properties

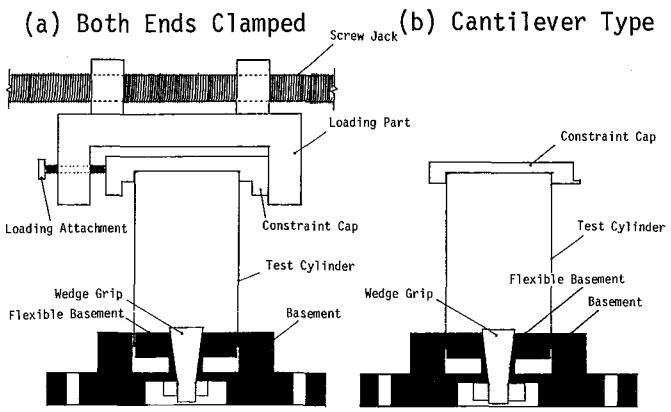

Fig.3: Boundary Condition

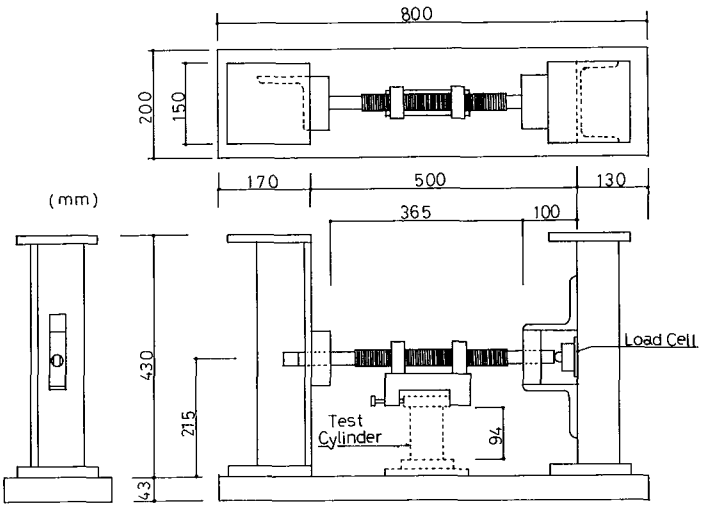

Fig.4: Loading Apparatus

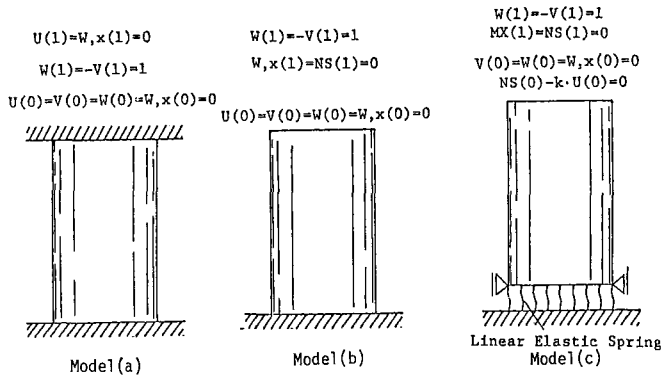

Fig.5: Boundary Vonditions for Linear Analysis

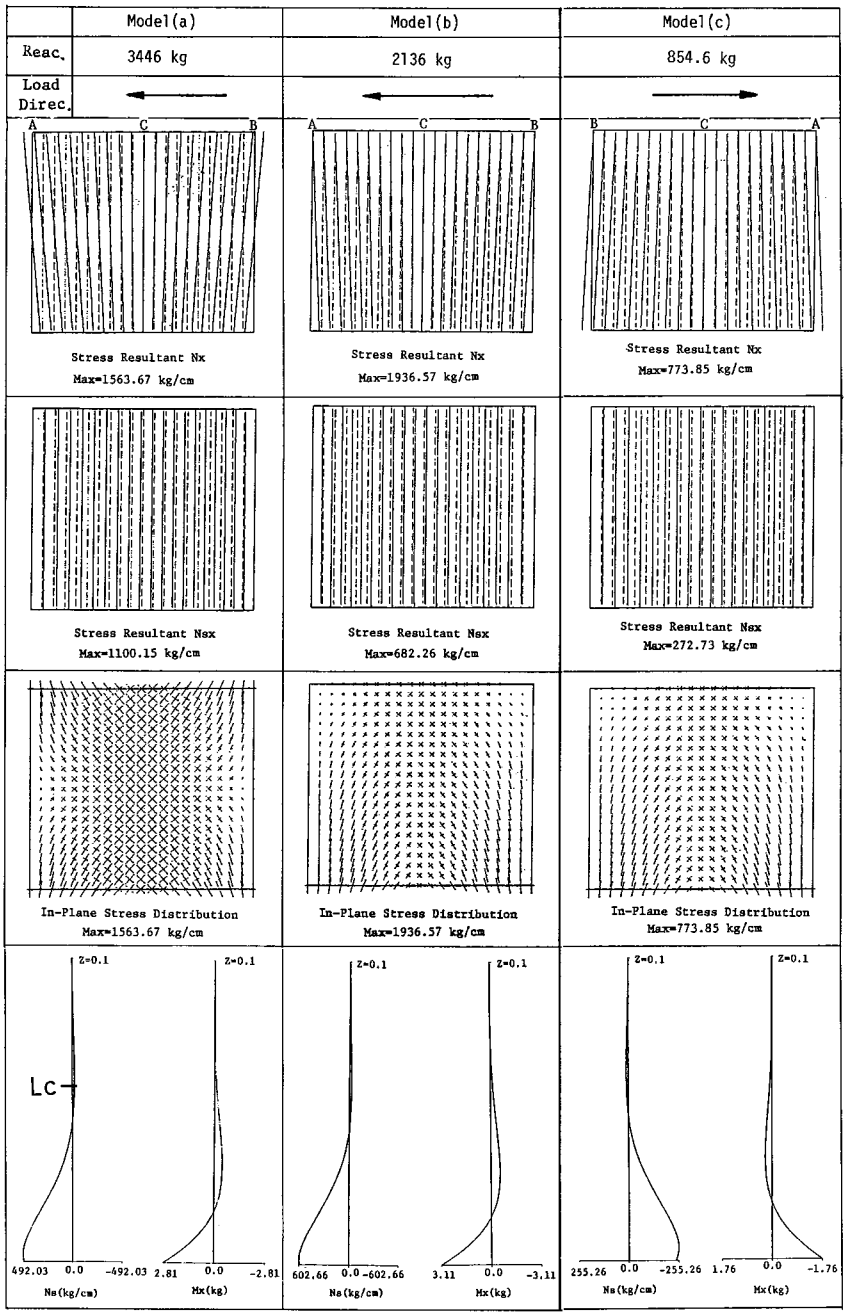

Fig.6: Results for the Prescrived Unit Displacement

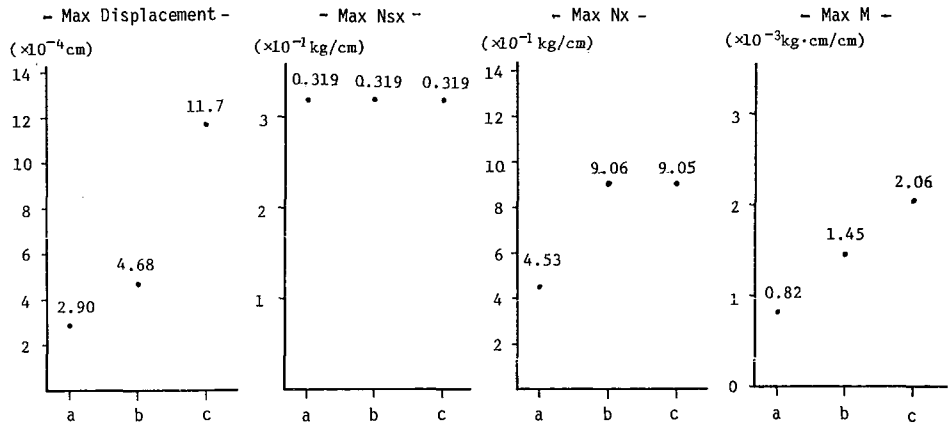

Fig.7: Maximum Values for the Unit Load

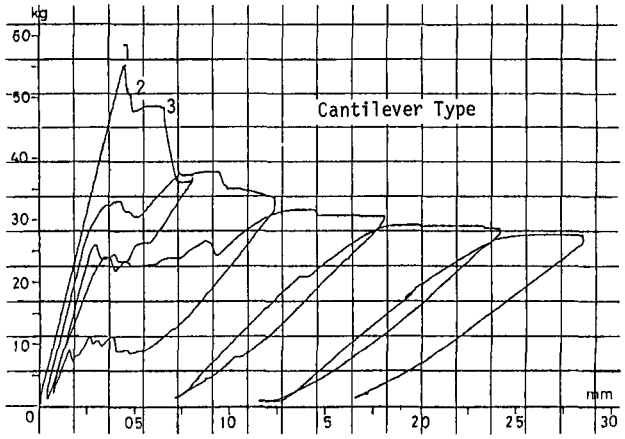

Fig.8: Realtion between Load and Displacement of the Top

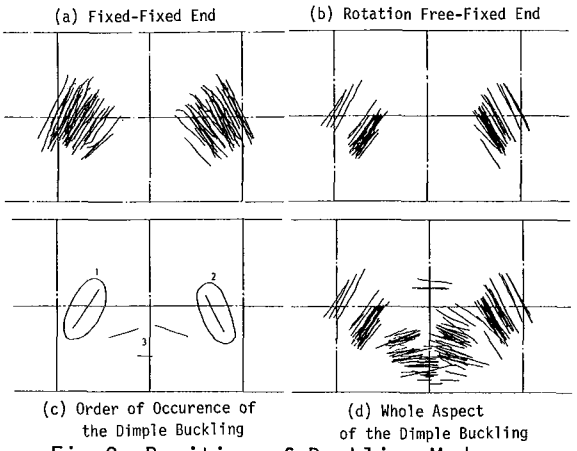

Fig.9: Position of Buckling Modes

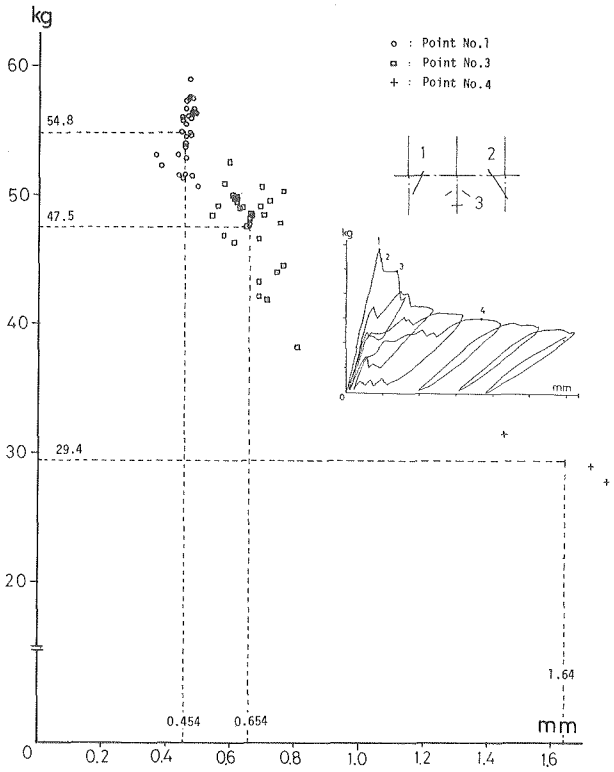

Fig.10: Distribution of Load and Displacement

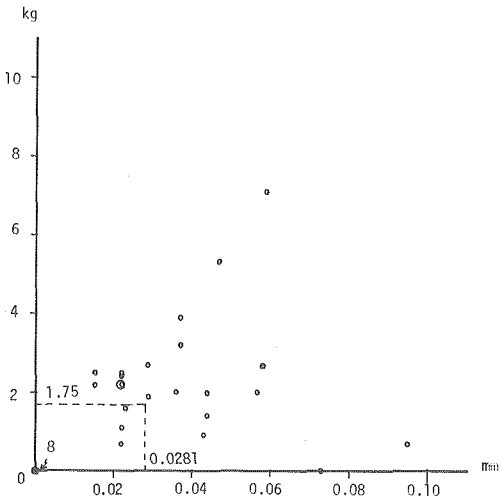

Fig.11: Difference of Appearance of Shear Buckling

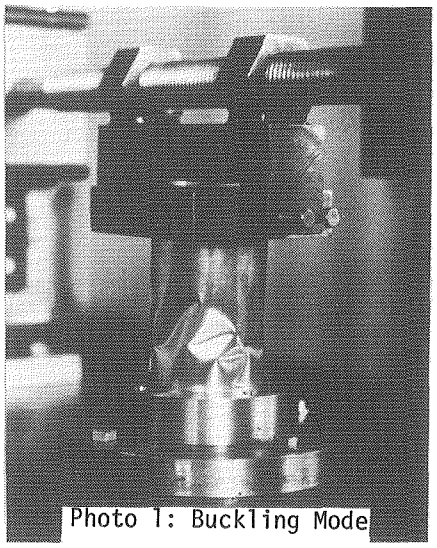

Photo 1: Buckling Mode